390573-3-T

ON THE SOLUTION OF THE E-FIELD INTEGRAL EQUATION: PART II

J. L. Volakis
J.-M. Jin
L. C. Kempel
D. C. Ross

Northrop Corporation
8900 E. Washington Blvd.
Pico Rivera CA 90660-3737

October 1991

390573-3-T = RL-2578

390573-3-T

ON THE SOLUTION OF THE E-FIELD INTEGRAL EQUATION: PART II

J. L. Volakis
J.-M. Jin
L. C. Kempel
D. C. Ross

Northrop Corporation
8900 E. Washington Blvd.
Pico Rivera CA 90660-3737

October 1991

On the Solution of the E-field Integral Equation — Part II

J.L. Volakis, J.-M. Jin, L.C. Kempel, and D.C. Ross

October 1991

Abstract

In a previous report [1], we derived an E-field integral equation for the scattering from resistive cards. Current and charge integral equations were developed using linear and doublet basis functions, respectively, and both formulations were shown to yield identical results for flat strips. In this follow-up report, we extend these formulations to arbitrary curved strips and reformulate the charge integral equation for solution using pulse basis. Of the presented current and charge integral equations, both have a field matrix time of $O(N^2)$. In addition, new results are presented for the S-shaped surface which illustrate that a small surface blemish can cause significant scattering returns at near grazing incidences.

1 Introduction

In a previous report [1] we derived a version of the E-field integral equation for scattering by resistive cards (see Figs. 1 and 2) in terms of the charge density rather than the current density as is usually done. The resulting charge integral equation was then solved for a flat strip via Galerkin's method using doublet basis functions, and it was shown that the resulting system was identical to that obtained from the current integral equation in conjunction with linear basis and Galerkin's testing. In this follow-up report the same integral equations are implemented via Galerkin's method for a curved resistive strip. Linear basis are employed for the current integral equation (see Fig. 3) and the resulting matrix elements are developed in detail. The charge integral equation is implemented using pulse basis to yield the same accuracy as the current integral equation with linear basis but because of the simplicity of pulse basis, the charge integral equation leads to a simpler implementation. In this case, however, the standard Galerkin's method (where the test pulse is the same as the expansion pulse) is not applicable because it leads to vanishing self cell elements for one of the two integrals in the equations. To avoid this, the test pulses are shifted one-half segment width but since the integrands are slowly varying over the test pulse, it was found sufficient to sample at two symmetric location over the test pulse. This makes the implementation of the charge integral equation rather simple and provided the CPU time for generating the matrix is maintained at $O(N^2)$, where N denotes the number subdivisions, the charge integral equation is more attractive. A way to achieve this is discussed and results are presented which demonstrate that the simpler charge equation is at least as efficient as the standard current integral equation. Further new results are presented for the scattering by the S-shaped surface which illustrates that a small blemish placed at the lower knee can cause substantial backscattering near edge-on incidence.

2 The integral equations

Referring to [1] and assuming the plane wave

$$\mathbf{H}^i = \hat{z} e^{jk_0(x\cos\phi_0 + y\sin\phi_0)} \tag{1}$$

to be incident upon the resistive strip shown in Figure 1, the pertinent current integral equations are

$$\begin{aligned} Y_0 E_s^i(s) &= RJ_s(s) + \frac{k_0}{4}\int_C J_{s'}(s')\left\{\hat{s}\cdot\hat{s}' H_0^{(2)}(k_0 r)\right\} ds' \\ &\quad + \frac{1}{4k_0}\int_C \frac{dJ_{s'}(s')}{ds'}\frac{\partial}{\partial s} H_0^{(2)}(k_0 r)\, ds' \end{aligned} \tag{2}$$

where $r = \sqrt{(x-x')^2 + (y-y')^2}$, $Y_0 = 1/Z_0$ is the free space admittance and $J_s(s)$ denotes the current density on the strip of resistivity R. Setting the charge density $\rho(s)$ as

$$\rho(s) = -\frac{\phi(s)}{j\omega} \tag{3a}$$

where

$$\phi(s) = \frac{dJ_s}{ds}, \tag{3b}$$

we can alternatively write (2) as

$$\begin{aligned} Y_0 E_s^i(s) &= RJ_s(s) - \frac{k_0}{4}\int_C \phi(s') G_I(x,y;x',y')\, ds' \\ &\quad + \frac{1}{4k_0}\int_C \phi(s')\frac{\partial}{\partial s} H_0^{(2)}(k_0 r)\, ds', \end{aligned} \tag{4}$$

which is the charge integral equation. In this

$$G_I(x,y;x',y') = \int_0^{s'} (\hat{s}\cdot\hat{s}'') H_0^{(2)}(k_0\tilde{r})\, ds'', \tag{5}$$

$$\tilde{r} = \sqrt{(x-x'')^2 + (y-y'')^2}, \tag{6}$$

and it can be shown (see Appendix) that

$$\begin{aligned} J_s(s) &= -\frac{1}{2}\int_C \left(\frac{L-2\delta}{L}\right)[\phi(s+\delta)-\phi(s-\delta)]\,d\delta \\ &= -\frac{1}{2}\left\{\int_s^{L/2+s}\left[1-\frac{2(s'-s)}{L}\right]\phi(s')\,ds' \right. \\ &\quad \left. -\int_{-L/2+s}^{s}\left[1+\frac{2(s'-s)}{L}\right]\phi(s')\,ds'\right\} \end{aligned} \tag{7}$$

with L denoting the length of the strip and s' is the cumulative distance along the strip up to the point (x', y'). Substitution of (7) into (4) then leads to an integral equation only in terms of the charge density $\phi(s')$.

3 Galerkin's Solution of the Current Integral Equation for an Arbitrary Surface Using Linear Basis

Consider now an arbitrarily curved strip or a closed cylinder, shown in Fig. 4, whose surface satisfies the resistive sheet condition. The excitation is a plane wave and we are interested in the solution of the surface current density $J_s(s)$, where s is a measure of the distance along the cylinder's or strip's contour. Hereon, $\hat{s}$ will denote the unit vector tangent to the resistive surface.

To discretize the integral equation (2), the surface is subdivided into straight segments as shown in Fig. 5 and as in the case of the flat strip we again choose the expansion and testing functions to be the triangle functions shown in Fig. 3(a). To define these more explicitly, let us assume that one of them is centered at the node (x_m, y_m), as shown in Fig. 6, with the left and right segments being of length

$$\begin{aligned} s_{m_1} &= \sqrt{(x_m - x_{m-1})^2 + (y_m - y_{m-1})^2} \\ s_{m_2} &= \sqrt{(x_{m+1} - x_m)^2 + (y_{m+1} - y_m)^2} \end{aligned} \tag{8}$$

respectively. We can then express $W_m(s)$ and $L_m(s)$ as

$$W_m(s) = L_m(s) = \begin{cases} \dfrac{s}{s_{m1}} & 0 < s < s_{m1} \\ \dfrac{s_{m2} - s}{s_{m2}} & 0 < s < s_{m2} \end{cases} \tag{9}$$

which are suitable for integration along the s coordinate. In the subsequent calculations we shall also make use of the parameters

$$\theta_{m1} = \tan^{-1}\left(\frac{y_m - y_{m-1}}{x_m - x_{m-1}}\right), \tag{10}$$

$$\theta_{m2} = \tan^{-1}\left(\frac{y_{m+1} - y_m}{x_{m+1} - x_m}\right), \tag{11}$$

$$\hat{s}_{m1} = \hat{x}\cos\theta_{m1} + \hat{y}\sin\theta_{m1}, \tag{12}$$

$$\hat{s}_{m2} = \hat{x}\cos\theta_{m2} + \hat{y}\sin\theta_{m2}, \tag{13}$$

where the last expressions represent unit vectors which are tangent to the segment on either side of the point (x_m, y_m). Using these parameters, the parametric equations for the linear segment to the left of (x_m, y_m) are

$$x = x_{m-1} + s\cos\theta_{m1}, \quad y = y_{m-1} + s\sin\theta_{m1}, \tag{14}$$

and those for the segment to the right of (x_m, y_m) are

$$x = x_m + s\cos\theta_{m2}, \quad y = y_m + s\sin\theta_{m2}. \tag{15}$$

Thus, given N samples of the strip's or cylinder's surface we can proceed with the computation of all parameters describing the linear segment which make the discrete version of that surface.

Substituting (9) into (2) we obtain the discrete system

$$[A_{mn}]\,[J_n] = [b_m] \tag{16}$$

where the elements of the matrix $[A_{nm}]$ and those of the excitation column can be defined in terms of the parameters introduced in (10)– (15). For the

excitation matrix elements we have

$$\begin{aligned} b_n &= (\sin\phi_0\cos\theta_{n1} - \cos\phi_0\sin\theta_{n1}) \\ &\quad \cdot \int_0^{s_{n1}} \frac{s}{s_{n1}} e^{jk_0\{(x_{n-1}+s\cos\theta_{n1})\cos\phi_0+(y_{n-1}+s\sin\theta_{n1})\sin\phi_0\}}\, ds \\ &\quad + (\sin\phi_0\cos\theta_{n2} - \cos\phi_0\sin\theta_{n2}) \\ &\quad \cdot \int_0^{s_{n2}} \frac{s_{n2}-s}{s_{n2}} e^{jk_0\{(x_n+s\cos\theta_{n2})\cos\phi_0+(y_n+s\sin\theta_{n2})\sin\phi_0\}}\, ds \end{aligned} \tag{17}$$

which after integration can be written as

$$\begin{aligned} b_n &= \frac{1}{s_{n1}}(\sin\phi_0\cos\theta_{n1} - \cos\phi_0\sin\theta_{n1})\, e^{jk_0[x_{n-1}\cos\phi_0+y_{n-1}\sin\phi_0]} \\ &\quad \cdot \left[\frac{e^{jk_0 s g_{n1}}}{-k_0^2(g_{n1})^2}(jk_0 g_{n1} - 1)\right]_0^{s_{n1}} \\ &\quad + \frac{1}{s_{n2}}(\sin\phi_0\cos\theta_{n2} - \cos\phi_0\sin\theta_{n2})\, e^{jk_0(x_n\cos\phi_0+y_n\sin\phi_0)} \\ &\quad \cdot \left[\frac{s_{n2}e^{jk_0 s g_{n2}}}{jk_0 g_{n2}} + \frac{e^{jk_0 s g_{n2}}}{k_0^2(g_{n2})^2}(jk_0 g_{n2} - 1)\right]_0^{s_{n2}} \end{aligned} \tag{18}$$

in which

$$g_{n1} = \cos\theta_{n1}\cos\phi_0 + \sin\theta_{n1}\sin\phi_0 \tag{19}$$

and g_{n2} is similarly defined upon replacing the subscripts in (19) from $n1$ to $n2$.

The impedance matrix elements can be expressed as

$$A_{nm} = a_{nm}^1 + a_{nm}^2 + a_{nm}^2 \tag{20}$$

where

$$a_{nm}^1 = \int_{C_n} R(s)L_m(s)W_n(s)\, ds, \tag{21}$$

$$a_{nm}^2 = \frac{k_0}{4}\int_{C_n} W_n(s)\int_{C_m} L_m(s')\left\{(\hat{s}\cdot\hat{s}')H_0^{(2)}(k_0 r)\right\} ds'\, ds, \tag{22}$$

$$a_{nm}^3 = \frac{-1}{4k_0}\int_{C_n}\frac{dW_n(s)}{ds}\int_{C_m}\frac{dL_m(s')}{ds'}H_0^{(2)}(k_0 r)\, ds'\, ds. \tag{23}$$

The first of these integrals can be readily integrated once the resistivity is specified over the mth segment. Given that the resistivity will be discretely defined as a constant within each segment, with the mth segment defined as that between the $(m-1)$th and mth node, it follows that

$$a_{nm}^{1} = \begin{cases} R_n\left(\frac{s_{n1}}{3}\right) + R_{n+1}\left(\frac{s_{n2}}{3}\right) & n = m \\ \frac{R_n s_{n1}}{6} & n = m+1 \\ \frac{R_m s_{m1}}{6} & n = m-1 \\ 0 & \text{otherwise,} \end{cases} \tag{24}$$

where R_m denotes the average resistivity of the mth segment.

To evaluate a_{mn}^{2} we proceed with the substitution of the expansion and weighting functions as given in (9). Doing so we obtain

$$\begin{aligned} a_{nm}^{2} &= \frac{k_0}{4}(\hat{s}_{n1}\cdot\hat{s}_{m1})\int_0^{s_{n1}}\left\{\frac{s}{s_{n1}}\right\}\int_0^{s_{m1}}\left\{\frac{s'}{s_{m1}}\right\}H_0^{(2)}(k_0 r_{11})\,ds'\,ds \\ &\quad + \frac{k_0}{4}(\hat{s}_{n1}\cdot\hat{s}_{m2})\int_0^{s_{n1}}\left\{\frac{s}{s_{n1}}\right\}\int_0^{s_{m2}}\left\{\frac{s_{m2}-s'}{s_{m2}}\right\}H_0^{(2)}(k_0 r_{12})\,ds'\,ds \\ &\quad + \frac{k_0}{4}(\hat{s}_{n2}\cdot\hat{s}_{m1})\int_0^{s_{n2}}\left\{\frac{s_{n2}-s}{s_{n2}}\right\}\int_0^{s_{m2}}\left\{\frac{s'}{s_{m1}}\right\}H_0^{(2)}(k_0 r_{21})\,ds'\,ds \\ &\quad + \frac{k_0}{4}(\hat{s}_{n2}\cdot\hat{s}_{m2})\int_0^{s_{n2}}\left\{\frac{s_{n2}-s}{s_{n2}}\right\}\int_0^{s_{m2}}\left\{\frac{s_{m2}-s'}{s_{m2}}\right\}H_0^{(2)}(k_0 r_{22})\,ds'\,ds \\ &= a_{nm}^{21} + a_{nm}^{22} + a_{nm}^{23} + a_{nm}^{24}, \end{aligned} \tag{25}$$

where

$$\begin{aligned} r_{11} &= \Big[(x_{n-1} + s\cos\theta_{n1} - x_{m-1} - s'\cos\theta_{m1})^2 \\ &\quad + (y_{n-1} + s\sin\theta_{n1} - y_{m-1} - s'\sin\theta_{m1})^2\Big]^{\frac{1}{2}}, \end{aligned} \tag{26}$$

$$\begin{aligned} r_{12} &= \Big[(x_{n-1} + s\cos\theta_{n1} - x_{m} - s'\cos\theta_{m2})^2 \\ &\quad + (y_{n-1} + s\sin\theta_{n1} - y_{m} - s'\sin\theta_{m2})^2\Big]^{\frac{1}{2}}, \end{aligned} \tag{27}$$

$$r_{21} = \Big[(x_n + s\cos\theta_{n2} - x_{m-1} - s'\cos\theta_{m1})^2 + (y_n + s\sin\theta_{n2} - y_{m-1} - s'\sin\theta_{m1})^2\Big]^{\frac{1}{2}}, \quad (28)$$

$$r_{22} = \Big[(x_n + s\cos\theta_{n2} - x_m - s'\cos\theta_{m2})^2 + (y_n + s\sin\theta_{n2} - y_m - s'\sin\theta_{m2})^2\Big]^{\frac{1}{2}}. \quad (29)$$

All of the integrals in (25) can be evaluated numerically except when $n = m$ and $n = m \pm 1$. In this case some of the integrands become singular and although their singularity is integrable, the associated integrals must, nevertheless, be evaluated with care. When $n = m$, the integrand of the first (a_{nm}^{21}) and fourth (a_{nm}^{24}) integrals is singular at $s = s'$. To evaluate them we can rewrite a_{nm}^2 as in (27) of [1]. However, a more accurate procedure is to regularize the approximate integrands by adding and subtracting a term which can be integrated analytically. Applying this procedure to the first term of a_{nn}^2 gives

$$a_{nn}^{21} = \frac{k_0}{4}\int_0^{s_{n1}}\int_0^{s_{n1}}\left(\frac{s}{s_{n1}}\right)\left[\left(\frac{s'}{s_{n1}}\right)H_0^{(2)}(k_0|s-s'|) - \left(\frac{s'}{s_{n1}}\right)\frac{j2}{\pi}\ln\left(\frac{1}{2}k_0|s-s'|-1\right)\right]ds'\,ds + \frac{jk_0}{2\pi}\frac{(s_{n1})^2}{72}\left\{-35 + 24\ln\left(\frac{k_0 s_{n1}}{2}\right)\right\} \quad (30)$$

and for the fourth term we obtain

$$a_{nn}^{24} = \frac{k_0}{4}\int_0^{s_{n1}}\int_0^{s_{n1}}\left\{\frac{s_{n2}-s}{s_{n2}}\right\}\left[\left\{\frac{s_{n2}-s'}{s_{n2}}\right\}H_0^{(2)}(k_0|s-s'|) - \left\{\frac{s_{n2}-s'}{s_{n2}}\right\}\frac{j2}{\pi}\ln\left(\frac{1}{2}k_0|s-s'|\right)\right]ds'\,ds + \frac{jk_0}{2\pi}\left\{\frac{(s_{n2})^2}{144}\left(-61 + 48\ln\left(\frac{k_0}{2}\right) + 12\ln(s_{n2})\right) - \int_0^{s_{n2}}\left\{\frac{s_{n2}-s}{s_{n2}}\right\}^2(s-s_{n2})\ln|s-s_{n2}|\,ds\right\} \quad (31)$$

The integrands of all integrals appearing in (31) and (32) are now non-singular and can be evaluated numerically. We note that in obtaining the

analytical portions of (30) and (31) we employed the integral identities

$$\int_0^a \ln\left(c|x-x'|\right)\,dx' = a\ln(c) - a + x\ln|x| - (x-a)\ln|x-a| \tag{32}$$

and

$$\int x\ln|x-d|\,dx = \frac{1}{2}\left(x^2-d^2\right)\ln(x-d) - \frac{1}{2}d^2\left[\frac{x}{d} + \frac{1}{2}\left(\frac{x}{d}\right)^2\right] \tag{33}$$

The second (a_{nm}^{22}) and third (a_{nm}^{23}) term of a_{nm}^2 have singular integrands when $n = m+1$ and $n = m-1$, respectively. Regularizing their integrands as above yields

$$\begin{aligned} a_{(m+1)m}^{22} &= \frac{k_0}{4}\int_0^{s_{m2}}\int_0^{s_{m2}} \left\{\frac{s}{s_{m2}}\right\}\left[\left\{\frac{s_{m2}-s'}{s_{m2}}\right\} H_0\left(k_0|s-s'|\right)\right. \\ &\quad \left. - \left\{\frac{s_{m2}-s'}{s_{m2}}\right\}\frac{j2}{\pi}\ln\left(\frac{1}{2}k_0|s-s'|\right)\right] ds'\,ds \\ &\quad + \frac{jk_0}{2\pi}\left\{\frac{\left(s_{m2}\right)^2}{72}\left(-19+12\ln\left(\frac{k_0 s_{m2}}{2}\right)\right)\right\} \end{aligned} \tag{34}$$

$$\begin{aligned} a_{(m-1)m}^{23} &= \frac{k_0}{4}\int_0^{s_{n2}}\int_0^{s_{n2}} \left\{\frac{s_{n2}-s}{s_{n2}}\right\}\left[\left\{\frac{s'}{s_{n2}}\right\} H_0^{(2)}\left(k_0|s-s'|\right)\right. \\ &\quad \left. - \left\{\frac{s'}{s_{n2}}\right\}\frac{j2}{\pi}\ln\left(\frac{1}{2}k_0|s-s'|\right)\right) ds'\,ds \\ &\quad + \frac{jk_0}{2\pi}\left\{\frac{\left(s_{n2}\right)^2}{72}\left(-19+12\ln\left(\frac{k_0 s_{n2}}{2}\right)\right)\right\} \end{aligned} \tag{35}$$

It remains to evaluate the integrals belonging to the term a_{nm}^3 which appears in (23). We have that

$$\begin{aligned} a_{nm}^3 &= \frac{-1}{4k_0}\frac{1}{s_{n1}s_{m1}}\int_0^{s_{n1}}\int_0^{s_{m1}} H_0^{(2)}\left(k_0 r_{11}\right) ds'\,ds \\ &\quad + \frac{1}{4k_0}\frac{1}{s_{n1}s_{m2}}\int_0^{s_{n1}}\int_0^{s_{m2}} H_0^{(2)}\left(k_0 r_{12}\right) ds'\,ds \\ &\quad + \frac{1}{4k_0}\frac{1}{s_{n2}s_{m1}}\int_0^{s_{n2}}\int_0^{s_{m1}} H_0^{(2)}\left(k_0 r_{21}\right) ds'\,ds \\ &\quad - \frac{1}{4k_0}\frac{1}{s_{n2}s_{m2}}\int_0^{s_{n2}}\int_0^{s_{m2}} H_0^{(2)}\left(k_0 r_{22}\right) ds'\,ds \\ &= a_{nm}^{31} + a_{nm}^{32} + a_{nm}^{33} + a_{nm}^{34} \end{aligned} \tag{36}$$

where r_{mn} are the same as for a^2_{nm} and were defined in (26)–(29). As in the case of a^2_{nm}, all of these integrals can be evaluated numerically except when $n = m$ and $n = m \pm 1$. When $n = m$, the integrands of a^{31}_{nn} and a^{34}_{nn} are singular and by regularizing them we obtain the alternate expressions

$$\begin{aligned} a^{31}_{nn} &= \frac{-1}{4k_0}\frac{1}{(s_{n1})^2}\int_0^{s_{n1}}\int_0^{s_{n1}}\left[H_0^{(2)}(k_0|s-s'|)\right. \\ &\quad \left. -\frac{j2}{\pi}\ln\left(\frac{1}{2}k_0|s-s'|\right)\right]ds'\,ds \\ &\quad -\frac{1}{4k_0}\frac{1}{(s_{n1})^2}\frac{j2}{\pi}\left\{\frac{(s_{n1})^2}{2}\left(-3+2\ln\left(\frac{k_0}{2}\right)+2\ln(s_{n1})\right)\right\} \end{aligned} \quad (37)$$

and

$$\begin{aligned} a^{34}_{nn} &= \frac{-1}{4k_0}\frac{1}{(s_{n2})^2}\int_0^{s_{n2}}\int_0^{s_{n2}}\left[H_0^{(2)}(k_0|s-s'|)\right. \\ &\quad \left. -\frac{j2}{\pi}\ln\left(\frac{1}{2}k_0|s-s'|\right)\right]ds'\,ds \\ &\quad -\frac{1}{4k_0}\frac{1}{(s_{n2})^2}\frac{j2}{\pi}\left\{\frac{(s_{n2})^2}{2}\left(-3+2\ln\left(\frac{k_0}{2}\right)+2\ln(s_{n2})\right)\right\} \end{aligned} \quad (38)$$

These are now suitable for numerical evaluation. When $n = m + 1$, the second term of a^3_{nm} has a singular integrand and must be evaluated as

$$\begin{aligned} a^{32}_{(m+1)m} &= \frac{1}{4k_0}\frac{1}{(s_{m2})^2}\int_0^{s_{m2}}\int_0^{s_{m2}}\left[H_0^{(2)}(k_0|s-s'|)\right. \\ &\quad \left. -\frac{j2}{\pi}\ln\left(\frac{1}{2}k_0|s-s'|\right)\right]ds'\,ds \\ &\quad +\frac{1}{4k_0}\frac{1}{(s_{m2})^2}\frac{j2}{\pi}\left[\frac{(s_{m2})^2}{2}\left(-3+2\ln\left(\frac{k_0}{2}\right)+2\ln(s_{m2})\right)\right] \end{aligned} \quad (39)$$

Finally, when $n = m - 1$, the third term in (37) should be evaluated as

$$\begin{aligned} a^{33}_{(m-1)m} &= \frac{1}{4k_0}\frac{1}{(s_{n2})^2}\int_0^{s_{n2}}\int_0^{s_{n2}}\left[H_0^{(2)}(k_0|s-s'|)\right. \\ &\quad \left. -\frac{j2}{\pi}\ln\left(\frac{1}{2}k_0|s-s'|\right)\right]ds'\,ds \\ &\quad +\frac{1}{4k_0}\frac{1}{(s_{n2})^2}\frac{j2}{\pi}\left[\frac{(s_{n2})^2}{2}\left(-3+2\ln\left(\frac{k_0}{2}\right)+2\ln(s_{n2})\right)\right] \end{aligned} \quad (40)$$

By comparing (37)–(40) it is evident that $a^{32}_{(m+1)m} = -a^{31}_{mm}$ and that $a^{33}_{(m-1)m} = -a^{34}_{mm}$. We further note that the simpler result in (34) of [1] could be used for evaluating $a^{31}_{nn}, a^{34}_{nn}, a^{32}_{(m+1)m}$ and $a^{33}_{(m-1)m}$.

4 Solution of the Charge Integral Equation Using Pulse Bases

Let us again consider the curved strip or cylinder shown in Fig. 4. We are now interested in solving the charge integral equation for this geometry. To do so we shall use pulse basis for expanding the quantity $\phi(s)$ and not the doublet function used in [1]. Thus, the charge conservation requirement must now be imposed explicitly. At first this would appear to yield an overdetermined system of equations. However, the usual Galerkin's or point matching technique leads to ill-conditioned systems and cannot be employed in the standard manner. In particular, on using point matching (at the center of the segment), the self-cell term of the last integral (4) vanishes making this testing/weighting procedure completely inappropriate since it zeros the most important term of the integral equation. Also, the usual Galerkin's testing leads to a similar situation. To avoid this, we can shift the weighting/testing pulse one-half of a subdivision as shown in Fig. 7. This type of weighting retains the dominance of the self-cell term but leads to $N-1$ equations for open surfaces, if N denotes the number of expansions employed in the discretization of (4). Consequently, the natural condition for a unique solution of the charge distribution is the conservation of charge equation

$$\sum_{n=1}^{N} \phi_n = 0 \tag{41}$$

where $\phi_n/(-j\omega)$ denotes the charge amplitudes at the nth segment. That is, they appear in the expansion

$$\phi \simeq \sum_{n=1}^{N} \phi_n P(s - s_n) \tag{42}$$

where

$$P(s) = \begin{cases} 1 & s_{m-1} < s < s_m \\ 0 & \text{elsewhere} \end{cases} \tag{43}$$

with $s_0 = 0$. Alternatively, in the case of point matching the test point can be placed halfway between the segment midpoint and its beginning or end point.

To discretize (4) as stated above, we introduce (42) in place of $\phi(s)$ and this yields the integral equation

$$\begin{aligned} Y_0 E_s^{inc} &= RJ_s(s) - \frac{k_0}{4} \sum_{n=1}^{N} \phi_n \int_{s_{n-1}}^{s_n} G_I(x, y; x', y')\, ds' \\ &\quad + \frac{1}{4k_0} \sum_{n=1}^{N} \phi_n \int_{s_{n-1}}^{s_n} \frac{\partial}{\partial s} H_0^{(2)}(k_0 r)\, ds' \end{aligned} \tag{44}$$

To generate a system of equations from this, we shall employ a dual set of test points located one-fourth of the mth and $(m+1)$th segment lengths from either side of (x_m, y_m) as illustrated in Fig. 8. This testing procedure is simpler than the shifted pulse approach and should not compromise the accuracy of the solution in view of the reduced singularity of the kernels in (4) versus those in (2). That is, each equation to be generated will be the sum of the equations obtained by testing at $(x_{m-1/4}, y_{m-1/4})$ and $(x_{m+1/4}, y_{m+1/4})$, and consequently the resulting system will retain certain symmetry with respect to the sample points (x_m, y_m).

To generate the matrix elements of the system resulting from (44) we must evaluate the integrals

$$T_{1n}(x_t, y_t) = \int_{s_{n-1}}^{s_n} G_I(x_t, y_t; x', y')\, ds' \tag{45}$$

and

$$T_{2n}(x_t, y_t) = \int_{s_{n-1}}^{s_n} \frac{\partial}{\partial s} H_0^{(2)}(k_0 r_t)\, ds' \tag{46}$$

where $x_t = x_{m\pm 1/4}$, $y_t = y_{m\pm 1/4}$,

$$G_I(x_t, y_t; x', y') = \int_0^{s(x',y')} (\hat{s}_t \cdot \hat{s}'') H_0^{(2)}(k_0 \tilde{r}_t)\, ds'', \tag{47}$$

$$r_t = \sqrt{(x_t - x')^2 + (y_t - y')^2}, \tag{48}$$

$$\tilde{r}_t = \sqrt{(x_t - x'')^2 + (y_t - y'')^2}, \tag{49}$$

and $s(x, y)$ denotes the cumulative distance up to (x, y).

Assuming equal segment lengths Δs, T_{1n} can be approximated as

$$\begin{aligned} T_{1n}(x_t, y_t) &= \Delta s\, G_I(x_t, y_t; x_{n-1/2}, y_{n-1/2}) \\ &= \Delta s \sum_{p=2}^{n} \int_0^{s_p} (\hat{s}_t \cdot \hat{s}_{p1}) H_0^{(2)}(k_0 \tilde{r}_{tp})\, ds' \\ &= \Delta s \sum_{p=2}^{n} I_{1p}(x_t, y_t) \end{aligned} \tag{50}$$

where

$$s_p = \begin{cases} s_{p1} = \Delta s & p < n \\ \dfrac{s_{n1}}{2} = \dfrac{\Delta s}{2} & p = n \end{cases} \tag{51}$$

and

$$\tilde{r}_{tp} = \left\{ x_t - x_{p-1} - s' \cos\theta_{p1})^2 + (y_t - y_{p-1} - s' \sin\theta_{p1})^2 \right\}^{\frac{1}{2}} \tag{52}$$

It is important to note that in generating the coefficients of ϕ_n, it is not necessary to perform the entire summation in (50) for every n. Instead the nth coefficient should be generated by adding one term to the $(n-1)$th coefficient, thus retaining our $O(N^2)$ operation count to fill the matrix. Also, there is substantial overlap in computing the coefficients for each of the two testing points and this could be exploited to further reduce the CPU matrix fill time.

All of the integrals $I_{1p}(x_t, y_t)$ appearing in the sum (50) have well-behaved integrands except when $t = t_{1p} = p - 1/4$ or $t = t_{2p} = p + 1/4$. In this case the integrands are singular and $I_{1p}(x_t, y_t)$ must be evaluated analytically. We have $(p < n)$

$$\begin{aligned} I_{1p}(x_{t_{1p}}, y_{t_{1p}}) &= \int_0^{s_{p1}} H_0^{(2)}(k_0 |\tfrac{3}{4} s_{p1} - s'|)\, ds' \\ &= \int_{-\frac{s_{p1}}{4}}^{\frac{3}{4} s_{p1}} H_0^{(2)}(k_0 |s'|)\, ds' \\ &\approx \left\{ s - j\frac{2}{\pi} \left[s \ln\left(\frac{k_0 \gamma s}{2} \right) - s \right] \right\}_{-\frac{1}{4} s_{p1}}^{\frac{3}{4} s_{p1}} \end{aligned} \tag{53}$$

where $\gamma = 1.781$ is Euler's constant. Also

$$I_{1p}(x_{t_{2p}}, y_{t_{2p}}) = \int_0^{s_p} H_0^{(2)}(k_0 |\frac{s_{p2}}{4} - s'|)\, ds'$$

$$= \int_{\frac{s_{p2}}{4}}^{s_p - \frac{s_{p2}}{4}} H_0^{(2)}(k_0|s'|)\,ds$$

$$\approx \left\{ s - j\frac{2}{\pi}\left[s\ln\left(\frac{k_0\gamma s}{2}\right) - s \right] \right\}_{s_{p2}/4}^{s_p - s_{p2}/4} \tag{54}$$

where $s_{p2} = \Delta s$ and $s_p = \Delta s$ if $p < n$ or $s_p = \frac{\Delta s}{2}$ if $p = n$.

The evaluation of I_2 is rather straightforward. We have

$$\begin{aligned} T_{2n}(x_t, y_t) &= \int_0^{s_{n1}} \frac{\partial}{\partial s} H_0^{(2)}(k_0 r_{tn})\,ds' \\ &= -k_0 \int_0^{s_{n1}} \hat{s}_t \cdot \hat{r}_{tn} H_1^{(2)}(k_0 r_{tn})\,ds' \end{aligned} \tag{55}$$

where

$$r_{tn} = \left\{ (x_t - x_{n-1} - s'\cos\theta_{n1})^2 + (y_t - y_{n-1} - s'\sin\theta_{n1})^2 \right\}^{\frac{1}{2}} \tag{56}$$

and

$$\hat{r}_{tn} = \frac{(x_t - x_{n-1} - s'\cos\theta_{n1})\hat{x} + (y_t - y_{n-1} - s'\sin\theta_{n1})\hat{y}}{r_{tn}}. \tag{57}$$

For $t \neq n - \frac{1}{4}$ or $t \neq (n-1) + \frac{1}{4}$ the integrand of (55) is non-singular, and T_{2n} can then be evaluated numerically. When $t = t_{1n} = n - \frac{1}{4}$, T_{2n} becomes

$$\begin{aligned} T_{2n}(x_{t1n}, y_{t1n}) &= -\int_0^{S_{n1}} \frac{\partial}{\partial s'} H_0^{(2)}(k_0 r_{tn})\,ds' \\ &= -[H_0^{(2)}(k_0 r_{tn})]_0^{s_{n1}} \\ &= -\left[H_0^{(2)}\left(\frac{k_0\Delta s}{4}\right) - H_0^{(2)}\left(\frac{3k_0\Delta s}{4}\right) \right]. \end{aligned} \tag{58}$$

Similarly when $t = t_{2n} = (n-1) + \frac{1}{4}$ we have

$$\begin{aligned} T_{2n}(x_{t2n}, y_{t2n}) &= -\int_0^{S_{n2}} \frac{\partial}{\partial s'} H_0^{(2)}(k_0 r_{tn})\,ds' \\ &= -[H_0^{(2)}(k_0 r_{tn})]_0^{s_{n2}} \\ &= -\left[H_0^{(2)}\left(\frac{3k_0\Delta s}{4}\right) - H_0^{(2)}\left(\frac{k_0\Delta s}{4}\right) \right] \\ &= -T_{1n}(x_{t1n}, y_{t1n}). \end{aligned} \tag{59}$$

Finally, before completing the discretization of (44) it is necessary to also consider the integral given in (7). From the Appendix we find that

$$\begin{aligned} J_s(s_{m\pm 1/4}) &= \frac{1}{\Delta s}\sum_{n=1}^{N}\phi_n\left[-\frac{N}{2}\gamma_{mn}^{\pm}+(n+\tfrac{1}{2}-m\mp\tfrac{1}{4})\Delta s\right. \\ &\quad \left.+(N+1-n+\tfrac{1}{2}-m\mp\tfrac{1}{4})\Delta s\right] \\ &= \sum_{n=1}^{N}\phi_n B_{mn}^{\pm} \end{aligned}$$

with

$$\gamma_{nm}^{\pm}=\begin{cases} \Delta s & (n+\frac{1}{2}-m\mp\frac{1}{4}) > \frac{1}{2} \\ 2(n+\frac{1}{2}-m\mp\frac{1}{4})\Delta s & |n+\frac{1}{2}-m\mp\frac{1}{4}| < \frac{1}{2} \\ -\Delta s & n+\frac{1}{2}-m\mp\frac{1}{4} < \frac{1}{2}. \end{cases}$$

The matrix system resulting from (44) can now be written as

$$[Z_{mn}][\phi_n]=[V_m]$$

where

$$\begin{aligned} V_m &= Y_0[E_s^{inc}(x_{m-1/4},y_{m-1/4})+E_s^{inc}(x_{m+1/4},y_{m+1/4})] \\ Z_{mn} &= R[B_{mn}^{+}+B_{mn}^{-}]-\frac{k_0}{4}[T_{1n}(x_{m+1/4},y_{m+1/4})+T_{1n}(x_{m-1/4},y_{m-1/4})] \\ &\quad +\frac{1}{4k_0}[T_{2n}(x_{m+1/4},y_{m+1/4})+T_{2n}(x_{m-1/4},y_{m-1/4})]. \end{aligned}$$

Provided T_{1n} is computed via the recursive procedure noted above, the fill time of $[Z_{mn}]$ will be of $O(N^2)$.

5 Numerical Implementation

In this section we present some numerical results based on the solution of the systems given in sections 3 and 4. We have numerically verified that the two systems give identical numerical results and thus only patterns based on the solution of the current integral equation will be presented.

Figure 9 compares the bistatic echowidth at 2 GHz of a 4 cm square metallic cylinder as computed using a pulse basis-point matching moment method program and a linear basis moment method program which employed Galerkin's technique. Figure 10 illustrates a similar comparison for a circular cylinder of radius 5 cm also at 2 GHz. Clearly, the results based on the two formulations are identical validating the given formulations for metallic surfaces.

Let us now look at scattering results for resistive surfaces. As an example, let us consider the flat resistive strip. Figure 11 compares the backscatter patterns for a 5 cm strip at 2GHz having a normalized resistivity of $R = 1.1 - j0.2$. A similar result is given in figure 12 for a flat strip whose left side is metallic whereas the right side has a normalized resistivity of $R = 2$. Once again the agreement between the two different formulations serves as validation for resistive surfaces.

We have been very interested in simulating infinite structures with finite models. One method of hiding the undesirable edge of a finite structure is to gradually taper the resistivity of a strip. An example of this is shown in figure 13 where a metallic halfplane is modelled by a 100λ long tapered card whose normalized resistivity varies as

$$R(x) = 20\left[\frac{x}{100}\right]^{16} - 100 \leq x \leq 0 \tag{60}$$

In this figure, the scattering by the tapered card is compared to the known metallic halfplane diffraction coefficient. These results are also compared to those obtained by a range gating procedure which is used for removing the contribution from the trailing edge. The range gating procedure involved the computation of the scattered field from a 0.5m wide strip for 128 frequencies between 100MHz and 10GHz. By inverse Fourier transforming this data, one is then able to isolate and gate the first order contribution of the strip's unwanted edge. The shown pattern is simply obtained by

applying a Fourier transform to the gate profile for each observation angle. This technique is very effective for E-polarization but for H-polarization, we are still hampered at grazing incidence by the difficulties discussed by Hermann [2].

A more pertinent application of the code's range gating feature to this project is the analysis of S-shaped surfaces. Previous work [3,4] presented a uniform physical optics (PO) diffraction coefficient for this geometry and employed the pulse basis-point matching implementation of the current integral equation to validate the PO analysis. Because the scattering return from the S-shaped geometries is rather small in certain regions, it is of interest to re-examine this geometry using the more accurate program presented in this report. The particular S-shaped surface to be considered is shown in figure 14 and its frequency response was computed as described above and processed via inverse Fourier transformation at each angle. Figure 15 illustrates the resulting range profile at grazing incidence. The trailing edge is pronounced and we observe a non-local behavior about the inflection point. The inflection point behavior effects low frequency returns and is not as pronounced for E-polarization. Figure 16 illustrates the range profile after removing the contribution from the termination edges of the finite model which simulates the inflection surface. The scattering pattern resulting from a Fourier transformation of this gated profile(repeated for each angle) is shown in figure 17. Clearly, the scattering near grazing incidence is negligible. Nevertheless, it is important to note that the current distribution near the inflection region is not necessarily negligible. In fact, as shown in figure 18, the current distribution at grazing incidence is much larger than the PO current near the inflection point and it drops off rather rapidly to small values past the lower and upper knees. The presence of the strong current near the inflection point and at the knees implies that a small perturbation of the surface in that region could cause a substantial return by unbalancing the canceling contributions from the surface currents on the otherwise smooth surface.

This conjecture was examined by placing a small depression centered at the location of the lower knee corresponding to the peak of the range profile shown in figure 16, i.e. at $x = -6.8cm$. The actual depression was a groove 0.01 cm deep and 4 cm wide and because of its extremely small depth such a groove can be thought of as a small scratch(almost invisible

to the naked eye). At the computation frequency of 5 GHz, this groove is $\frac{1}{600}\lambda$ deep! Surprisingly, the numerical results for this blemished surface are substantially different in the non-specular region for H-polarization(the E-polarization was not affected by the blemish). In particular, as shown in figure 19 the H-polarization pattern from the blemished surface has a distinct lobe near grazing incidence. A similar pattern is given in figure 20 when the same blemish is placed on the upper knee at $x = 6.8cm$. A lobe again appears near 165 degrees which is not as broad as that caused by the blemish on the lower knee. Tests were performed to verify the validity of the patterns in figures 19 and 20 and interestingly the same patterns were generated by our older code which was based on a different formulation. This provided some confidence that the results are not caused by numerical inaccuracies. Results were examined when the blemish was placed at other locations and it was observed that these grazing lobes persisted but were of reduced strength. At this point, an interesting task would be to examine the effect of the groove shape and position on the scattering pattern. Certainly the position will play a major role on the scattering strength. Nevertheless, the smoothness and shape of the blemish will likely play a role as well.

Appendix: The current in terms of charges

Consider the integral expression (see [1])

$$J_s = -\frac{1}{2}\int_0^{L/2}\left(\frac{L-2\delta}{L}\right)[\phi(s+\delta)-\phi(s-\delta)]\,d\delta \tag{61}$$

where $\phi(s)$ represents a quantity proportional to the charge on a strip of length $L/2$ and J_s is the corresponding current density. In evaluating the integral, $\phi(s)$ must be assumed to satisfy the conditions

$$\phi(s) = \phi(-s) = \phi(L-s) \tag{62}$$

and consequently it can be considered as a periodic function of period L (see figure). Because $\phi(s) = \phi(-s)$, only the portion of $\phi(s)$ in the region

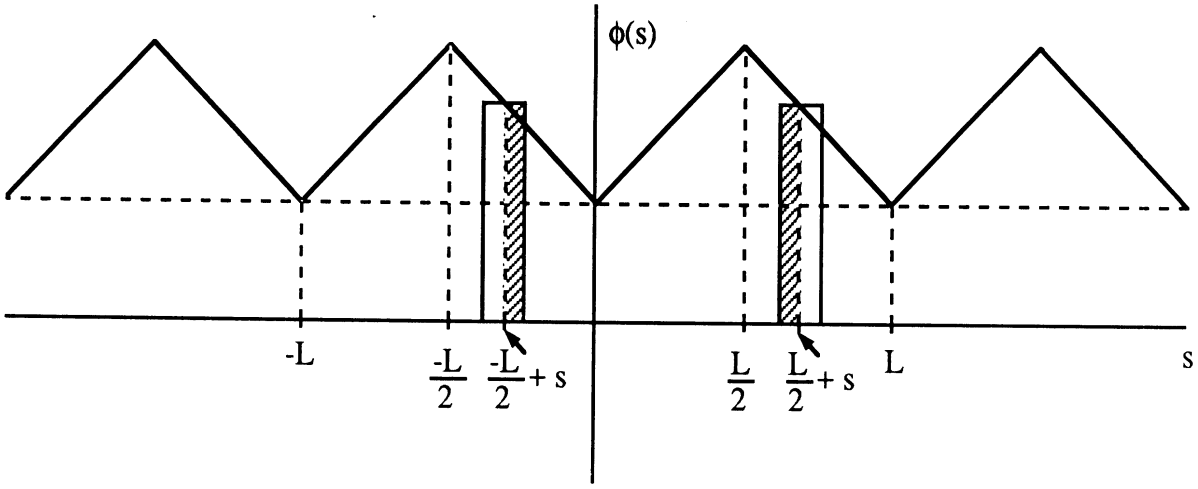

$0 < s < L/2$ is unique.

It is desirable to write (61) so that the integrand is a function of the unshifted $\phi(s)$. To this end, we write (61) as

$$J_s(s) = -\frac{1}{2}\int_0^{L/2}\left(1-\frac{2\delta}{L}\right)\phi(s+\delta)\,d\delta + \frac{1}{2}\int_{-L/2}^{0}\left(1+\frac{2\delta}{L}\right)\phi(s+\delta)\,d\delta$$

$$= -\frac{1}{2}\left\{\int_s^{L/2+s}\left[1-\frac{2(s'-s)}{L}\right]\phi(s')\,ds' + \int_{-L/2+s}^{s}\left[-1-\frac{2(s'-s)}{L}\right]\phi(s')\,ds'\right\} \quad (63)$$

Let us now assume that $\phi(s)$ can be expanded as a summation of pulses in the form

$$\phi(s) = \sum_{n=1}^{N}\phi_n P(s-s_n) \quad (64)$$

$$P(s-s_n) = \begin{cases} 1 & s_n-\Delta/2 < s < s_n+\Delta/2 \\ 0 & \text{elsewhere} \end{cases} \quad (65)$$

where N denotes the linear elements/segments comprising the $L/2$ long strip. Substituting (64) into (63) and making use of the relation $\phi(s) = \phi(-s) = \phi(L-s)$ yields

$$\begin{aligned} J_s(s_m) &= -\frac{1}{2}\int_0^{L/2}\left[E(s'-s_m)-\frac{2(s'-s_m)}{L}\right]\sum_{n=1}^{N}\phi_n P(s'-s_n)ds' \\ &\quad -\frac{1}{2}\int_{L/2}^{L/2+s}\left[1-\frac{2(s'-s_m)}{L}\right]\sum_{n=1}^{m^-}\phi_{N+1-n}P(s'-L/2-s_n)ds' \\ &\quad -\frac{1}{2}\int_{-L/2+s}^{0}\left[-1-\frac{2(s'-s_m)}{L}\right]\sum_{n=1}^{m^-}\phi_{N+1-n}P(s'+L/2-s_n)ds' \end{aligned} \quad (66)$$

In this

$$E(s'-s_m) = \left\{\begin{array}{ll} 1 & s'>s_m \\ & \\ -1 & s'<s_m \end{array}\right\} = U(s'-s_m) \quad (67)$$

and the upper summation limit $m^{\pm}$ implies that the integration of the pulse centered at $s_n \mp L/2$ with $|s_n - s_m| < \Delta/2$, will only be over a portion of it which corresponds to the crosshatched region in the figure.

From (66) and (65) we now have

$$\begin{aligned} J_s(s_m) &= -\frac{1}{2}\sum_{n=1}^{N}\phi_n I_n^{(1)}(s_m) - \frac{1}{2}\sum_{n=1}^{m^-}\phi_{N+1-n}I_n^{(2)}(s_m) \\ &\quad -\frac{1}{2}\sum_{n=m^+}^{N}\phi_{N+1-n}I_n^{(3)}(s_m) \end{aligned} \quad (68)$$

The integral $I_n^{(1)}(s_m)$ is given by

$$I_n^{(1)}(s_m) = \int_{s_n-\Delta/2}^{s_n+\Delta/2} U(s'-s_m)\,ds' - \frac{2}{L}\int_{s_n-\Delta/2}^{s_n+\Delta/2}(s'-s_m)\,ds'$$

where $U(s)$ denotes the unit step function, and can be evaluated to give

$$I_n^{(1)}(s_n) = \gamma(s_n - s_m) - \frac{2}{L}(s_n - s_m)\Delta \tag{69}$$

where

$$\gamma(s_n - s_m) = \begin{cases} \Delta & s_n - s_m > \Delta/2 \\ 2(s_n - s_m) & |s_n - s_m| < \Delta/2 \\ -\Delta & s_n - s_m < \Delta/2 \end{cases} \tag{70}$$

Similarly, the integrals $I_n^{(2)}(s_m)$ and $I_n^{(3)}(s_m)$ are given by

$$I_n^{(2)}(s_m) = \int_{s_n-\Delta/2}^{\ell_2(s_n,s_m)} ds' - \frac{2}{L}\int_{s_n-\Delta/2}^{\ell(s_n,s_m)} \left(\frac{L}{2} + s' - s_m\right) ds' \tag{71}$$

$$I_n^{(3)}(s_m) = \int_{\ell_3(s_n,s_m)}^{s_n+\Delta/2}(-1)\,ds' - \frac{2}{L}\int_{\ell_3(s_n,s_m)}^{s_n+\Delta/2} \left(s' - \frac{L}{2} - s_m\right) ds' \tag{72}$$

in which

$$\ell_2(s_n, s_m) = \begin{cases} s_n + \Delta/2 & s_n - s_m > \Delta/2 \\ s_m & |s_n - s_m| < \Delta/2 \end{cases} \tag{73}$$

and

$$\ell_3(s_n, s_m) = \begin{cases} s_n - \Delta/2 & s_n - s_m < \Delta/2 \\ s_m & |s_n - s_m| < \Delta/2. \end{cases} \tag{74}$$

Evaluating the integrals we obtain

$$I_n^{(2)}(s_m) = \begin{cases} -\dfrac{2}{L}(s_n - s_m)\Delta & s_n - s_m > \Delta/2 \\ \dfrac{(s_n - s_m - \Delta/2)^2}{L} & |s_n - s_m| < \Delta/2 \end{cases} \tag{75}$$

and

$$I_n^{(3)}(s_m) = \begin{cases} -\dfrac{2}{L}(s_n - s_m)\Delta & s_n - s_m < \Delta/2 \\ -\dfrac{(s_n - s_m + \Delta/2)^2}{L} & |s_n - s_m| < \Delta/2. \end{cases} \tag{76}$$

Using (75) and (76), the last two sums in (68) can be combined to yield

$$J_s(s_m) = -\frac{1}{2}\sum_{n=1}^{N} \phi_n I_n^{(1)}(s_m) - \frac{1}{2}\sum_{n=1}^{N} \phi_{N+1-n} I_n^{(4)}(s_m) \tag{77}$$

where

$$I_n^{(4)}(s_m) = I_n^{(2)}(s_m) + I_n^{(3)}(s_m) = -\frac{2}{L}(s_n - s_m)\Delta \tag{78}$$

More explicitly, $J_s(s)$ can be written as

$$J_s(s) = \frac{\Delta}{L}\sum_{n=1}^{N} \phi_n \left[-\frac{L}{2\Delta}\gamma(s_n - s) + (s_n - s) + (s_{N+1-n} - s) \right]. \tag{79}$$

Note that s can have any value and in fact it will be later chosen to be some distance away from s_n.

References

[1] John L. Volakis and Jian-Ming Jin, "On the Formulation and Solution of the E-field Integral Equation," University of Michigan Technical Report, 390573-2-T, 1991.

[2] Gabriel F. Herrmann, "Numerical Computation of Diffraction Coefficients," *IEEE Trans. Antennas Propagat.*,vol. AP-35, No. 1, pp. 53-61, 1987.

[3] Leo C. Kempel and John L. Volakis, "Numerical Simulation of the Scattering by S-shape Surfaces," University of Michigan Technical Report, 390285-1-T, 1990.

[4] J.L. Volakis, L.C. Kempel, and T.B.A. Senior, "A Uniform Physical Optics Approximation for Scattering by S-shaped Surfaces," University of Michigan Technical Report, 390285-2-T, 1990.

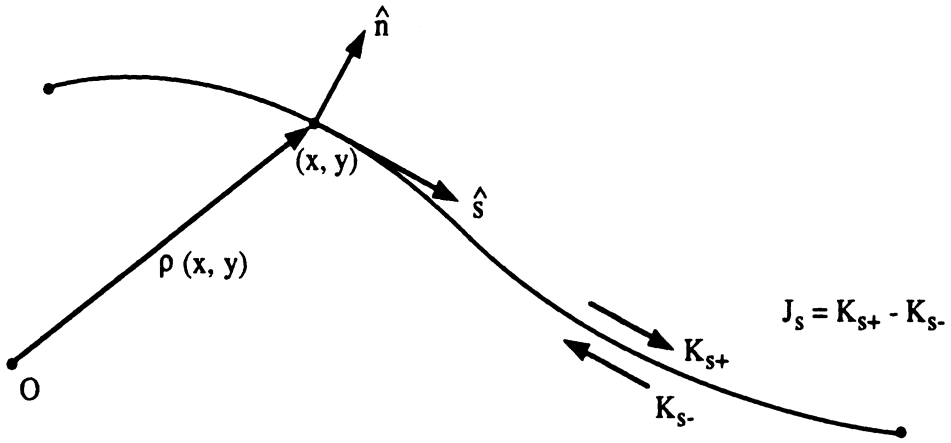

Figure 1. Geometry of the 2D curved surface (strip).

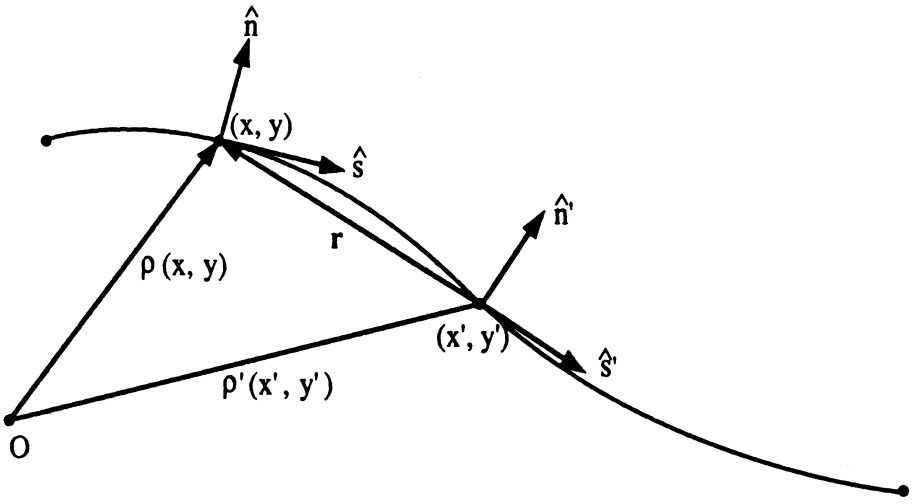

Figure 2. Illustration of the observation and integration point parameters.

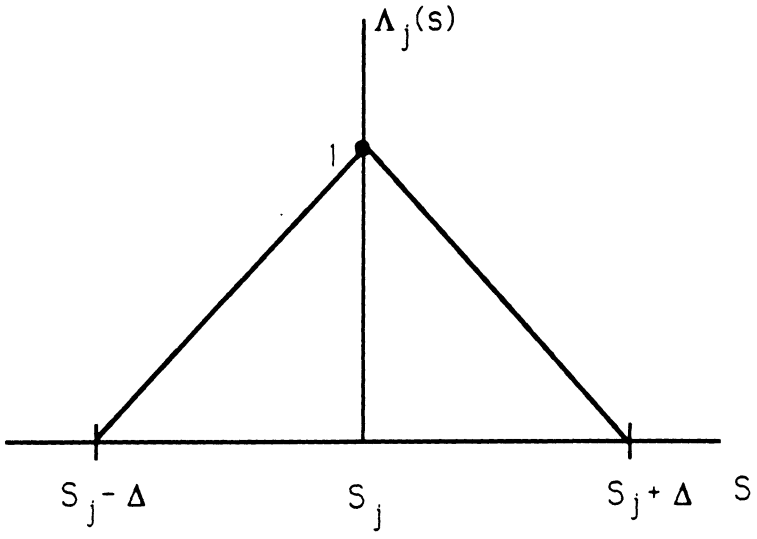

(a)

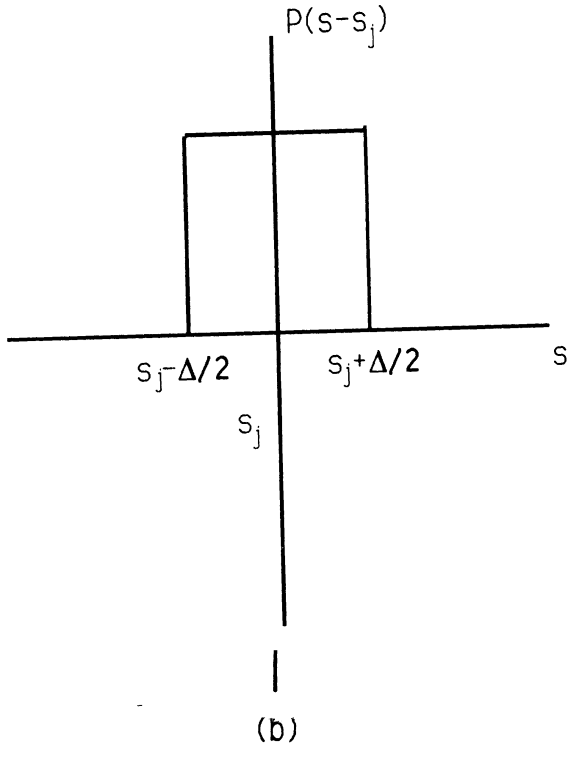

(b)

Figure 3. Expansion functions. (a) Linear expansion functions for the current (b) corresponding expansion functions for the charge.

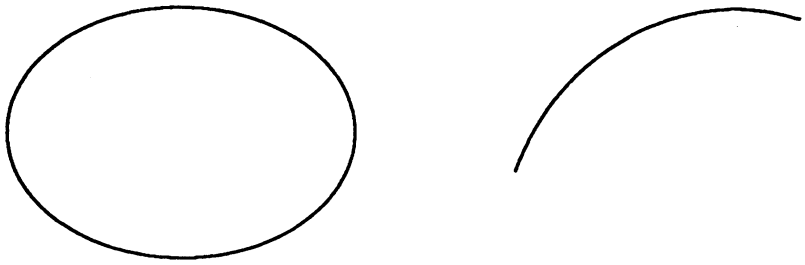

Figure 4. Illustration of an arbitrary cross section cylinder and a curved strip.

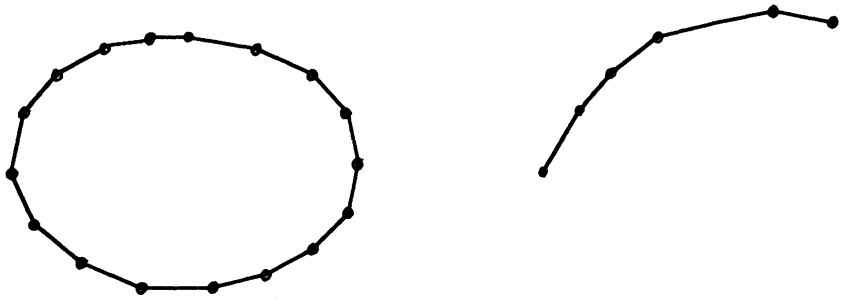

Figure 5. Discretized versions of the cylinder and the strip shown in Figure 4.

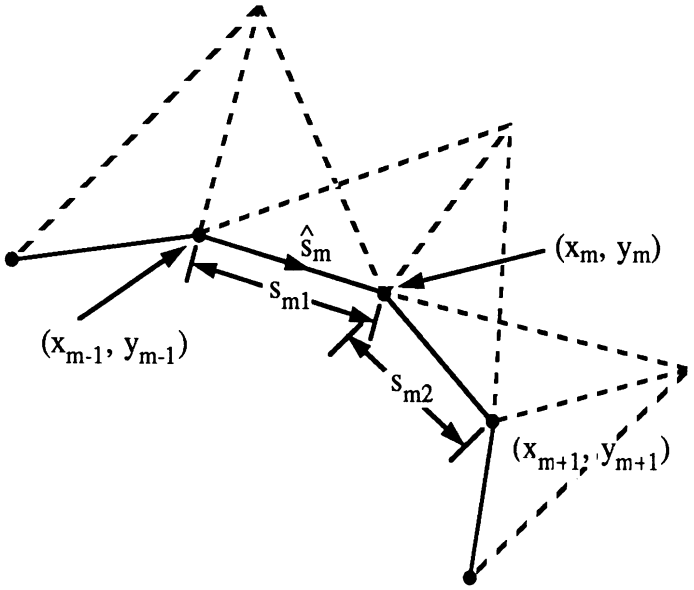

Figure 6. Geometrical parameters for adjacent segments.

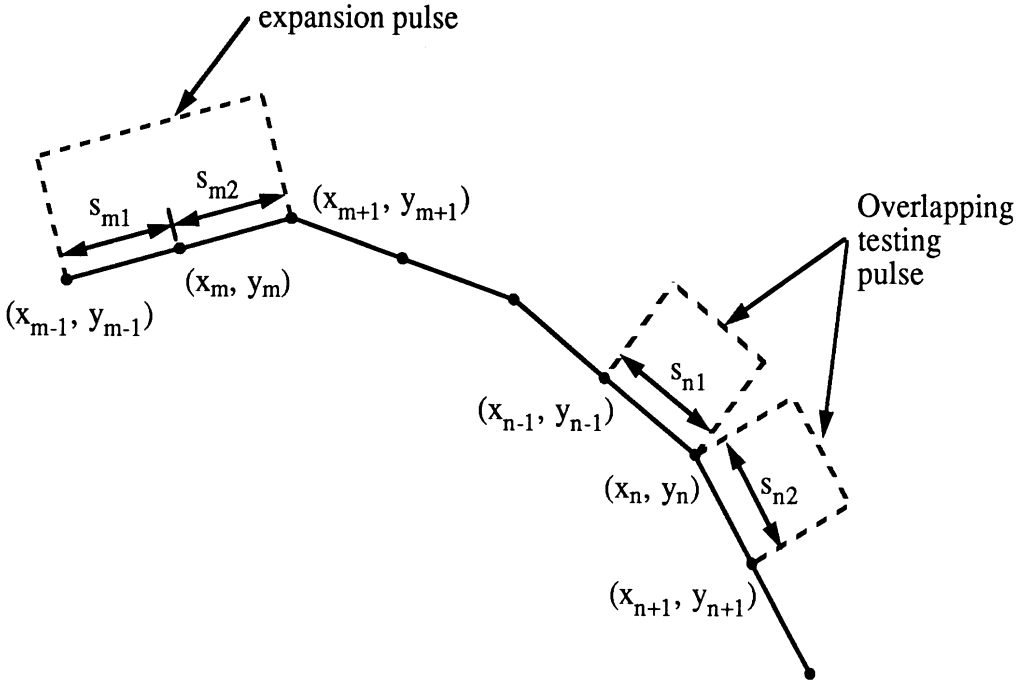

Figure 7. Illustration of discretization for pulse expansion and testing with shifted pulses.

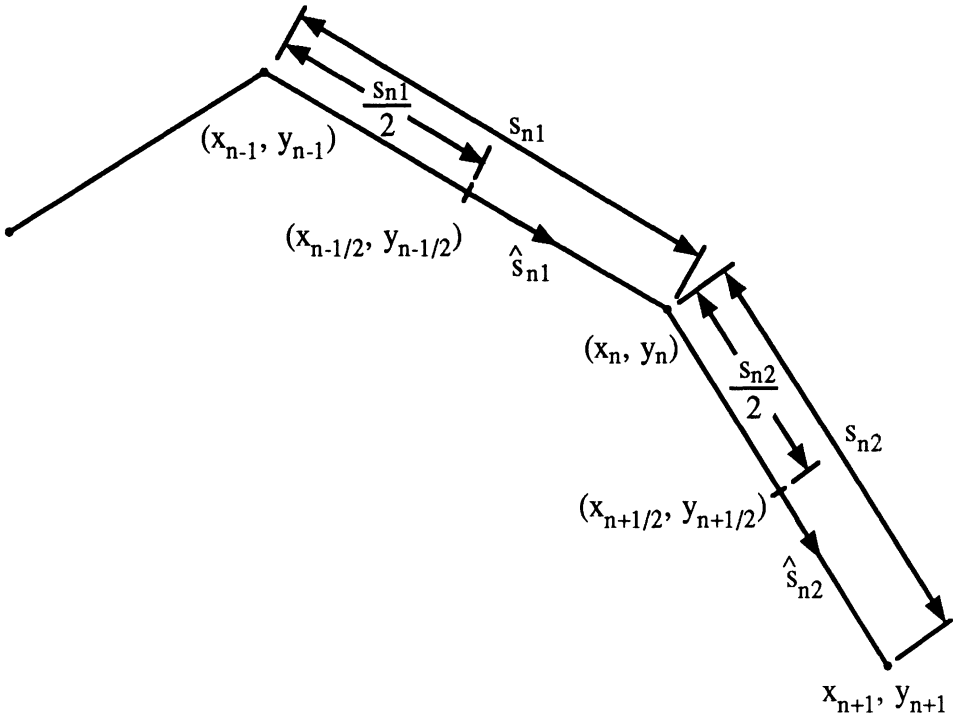

(a)

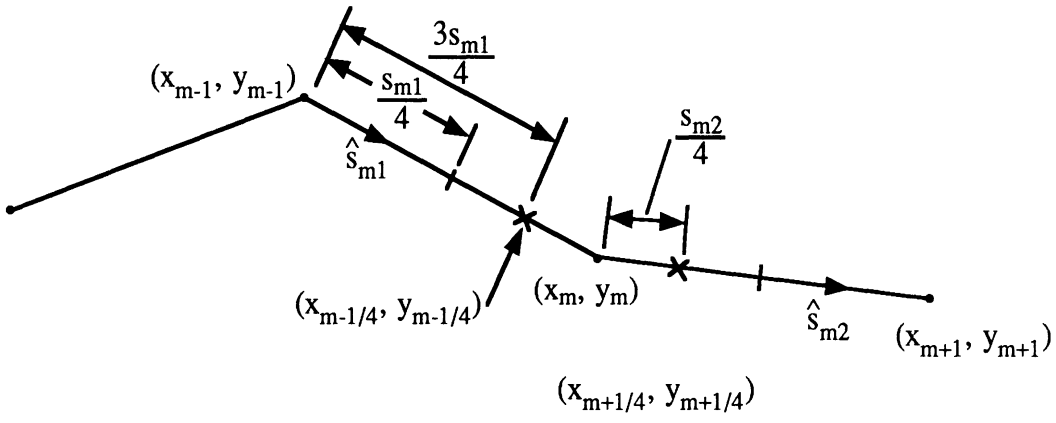

(b)

Figure 8. Illustration of parameters for pulse expansion and point matching in connection with the charge integral equation.

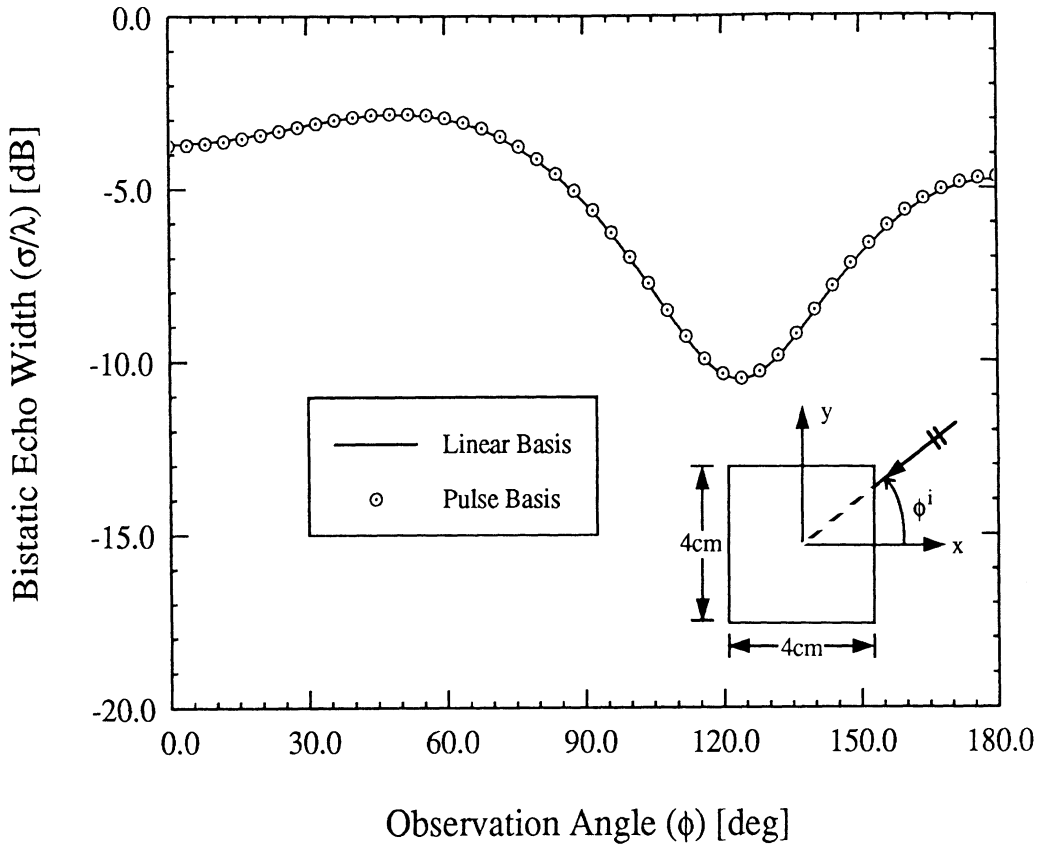

Figure 9. Bistatic echowidth of a 4cm square metallic cylinder computed with $\phi^i = 0$ and f = 2 GHz.

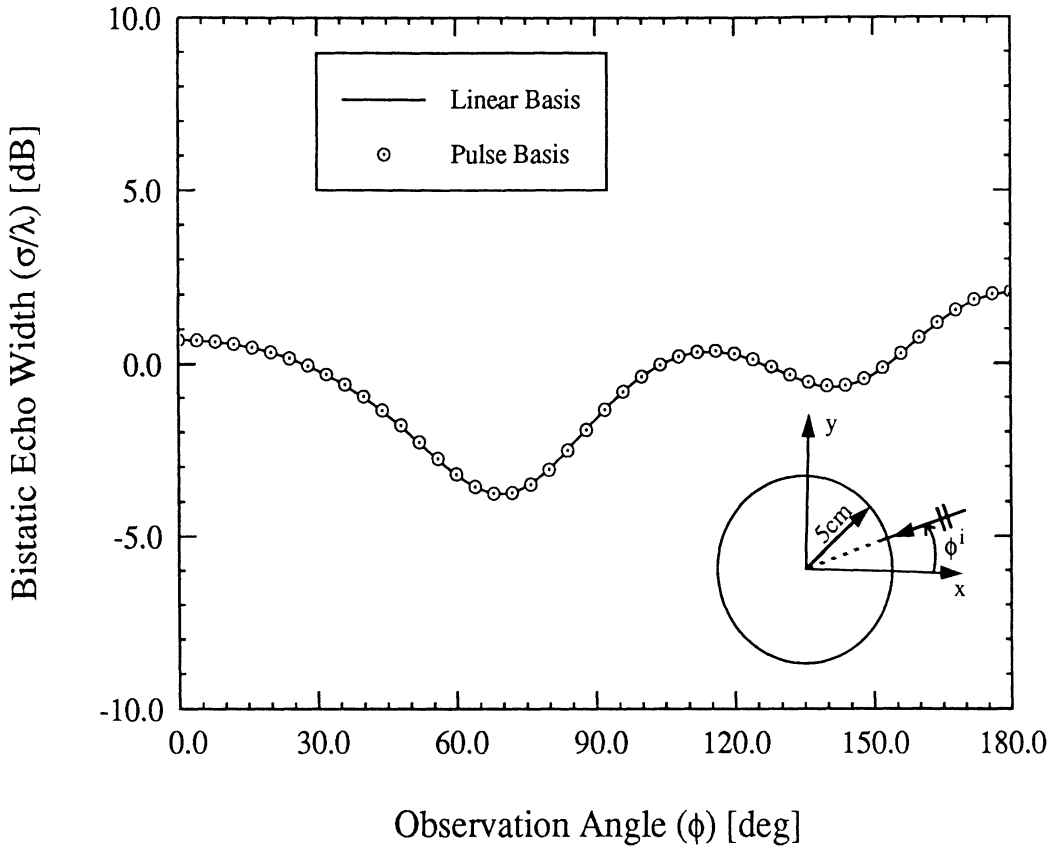

Figure 10. Bistatic echowidth at a 5cm metallic circular cylinder computed with $\phi^i = 0$ and f = 2 GHz.

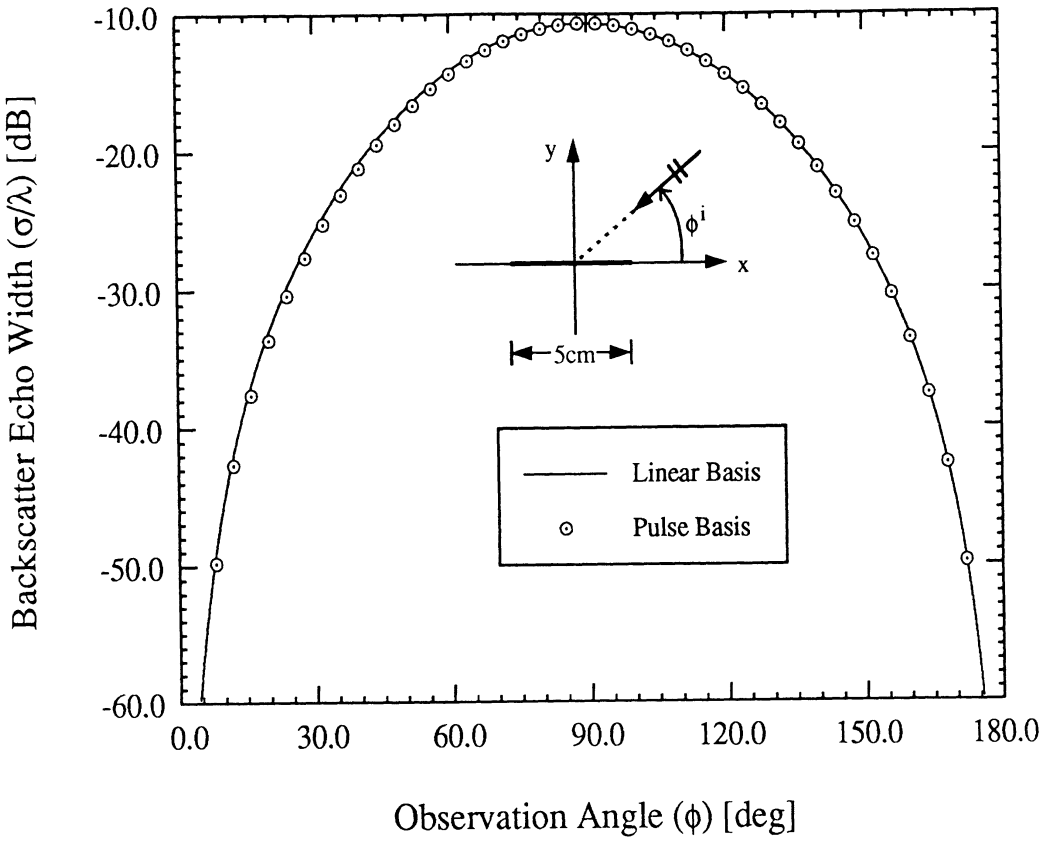

Figure 11. Backscatter echowidth of a 5cm resistive strip with normalized resistivity R = 1.1 + i0.2 computed at f = 2 GHz.

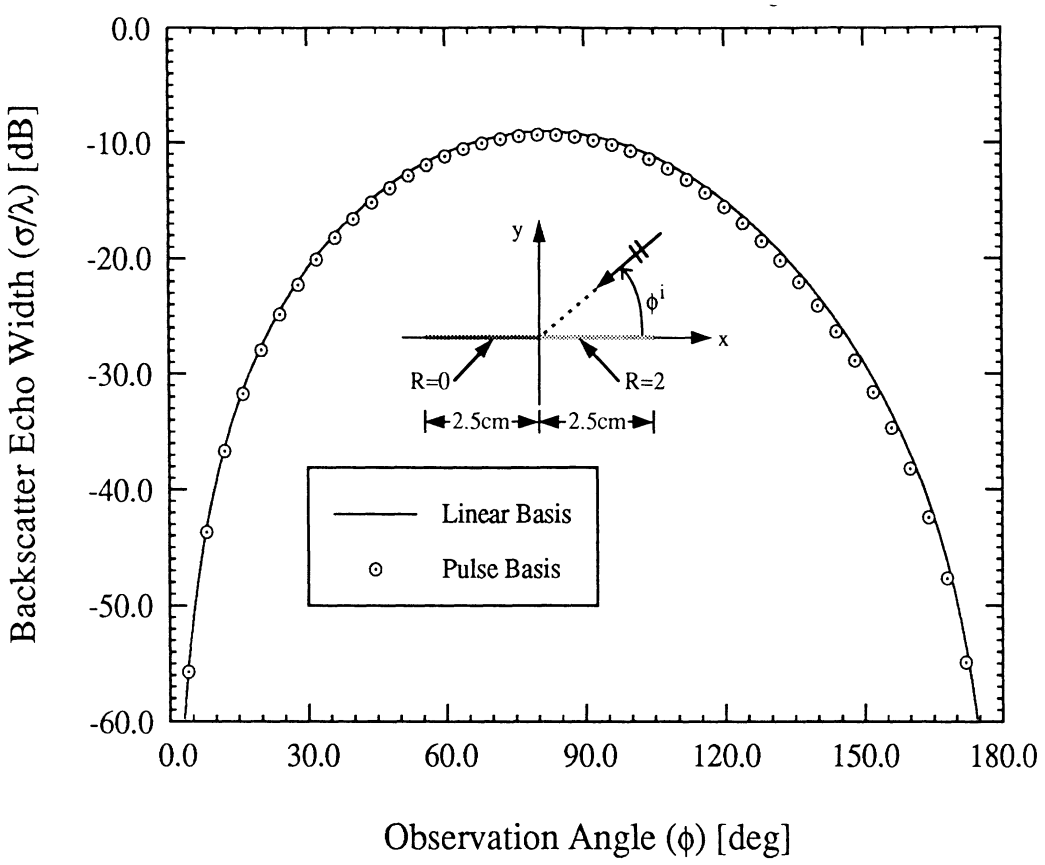

Figure 12. Backscatter echowidth of coplanar joined metallic and resistive strips each 2.5cm wide computed at f = 2 GHz.

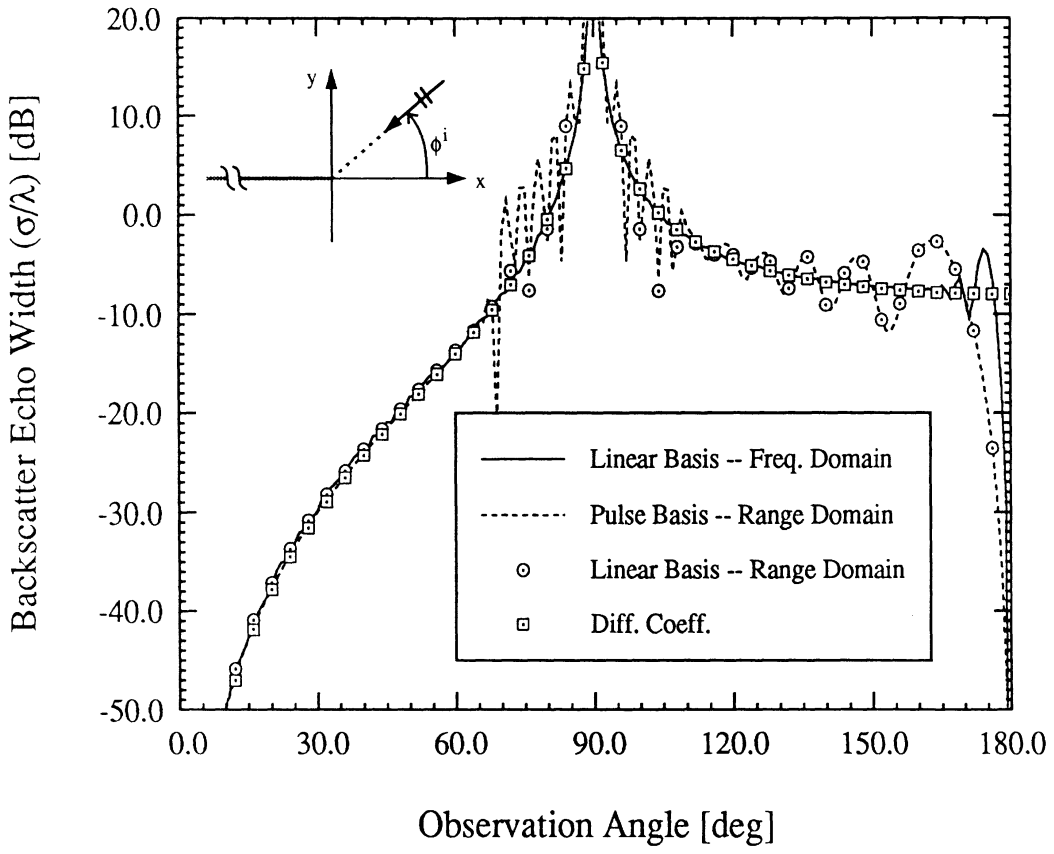

Figure 13. Backscatter echowidth of a simulated metallic halfplane whose trailing edge is suppressed by either a long tapered resistive card or by range gating.

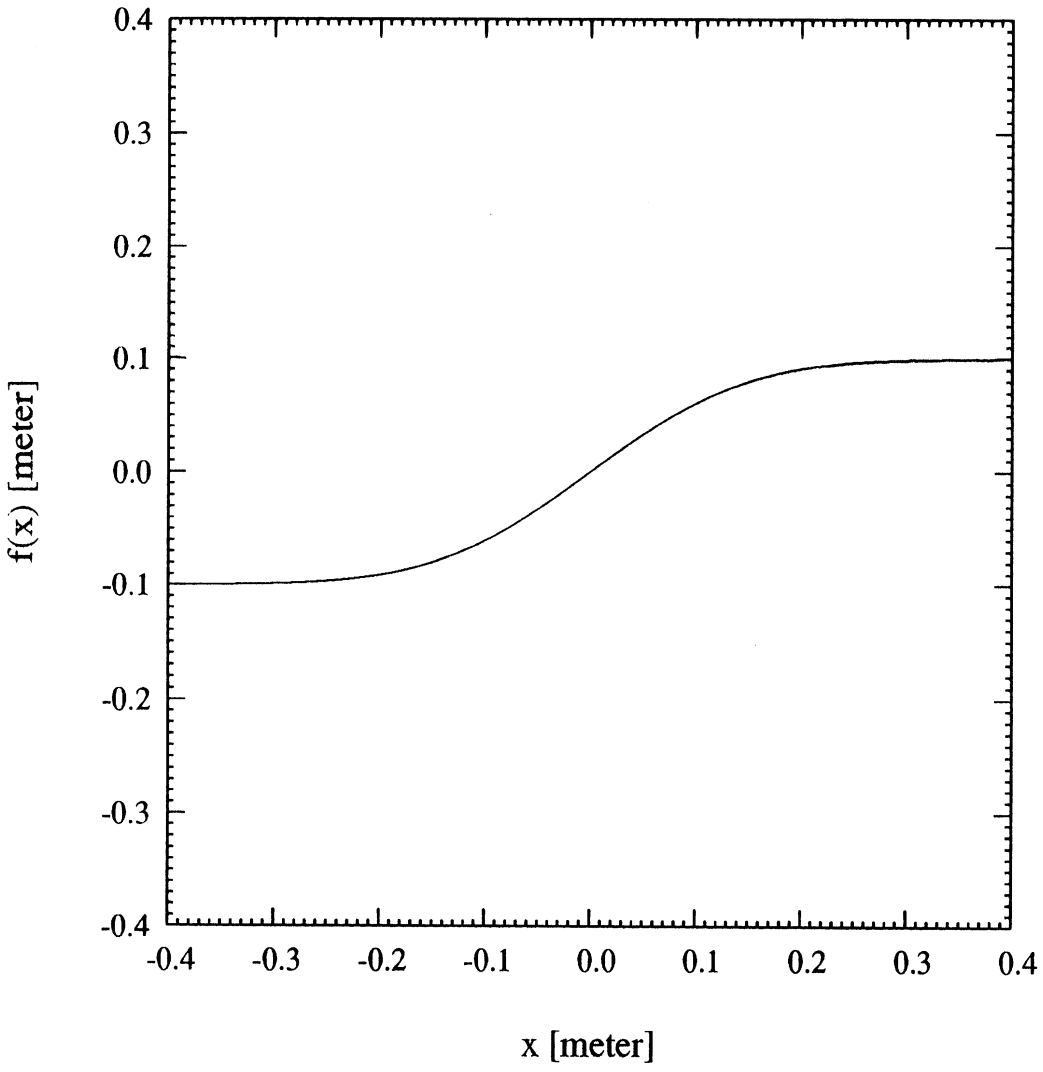

Figure 14. S-shaped surface which is described by $f(x) = 0.1\ \mathrm{erf}(6x)$.

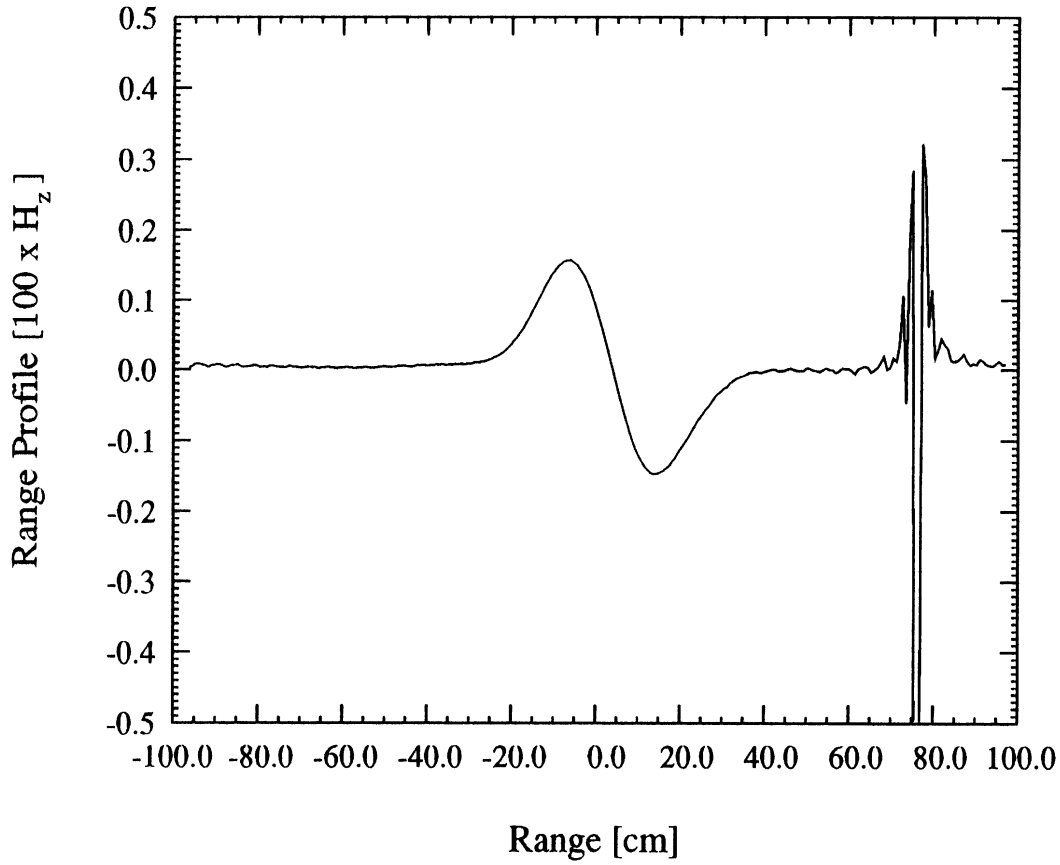

Figure 15. Range profile of the surface (see fig. 14) at grazing incidence.

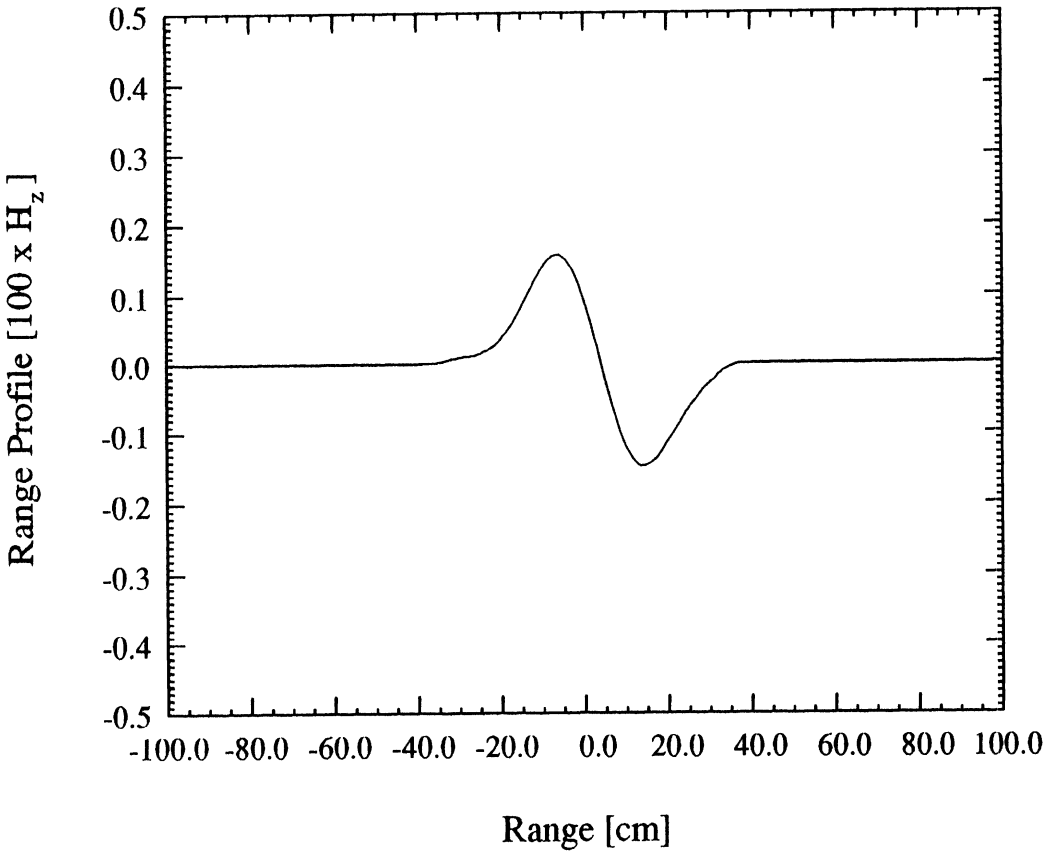

Figure 16. Gated range profile of the surface (see fig. 14) at grazing incidence.

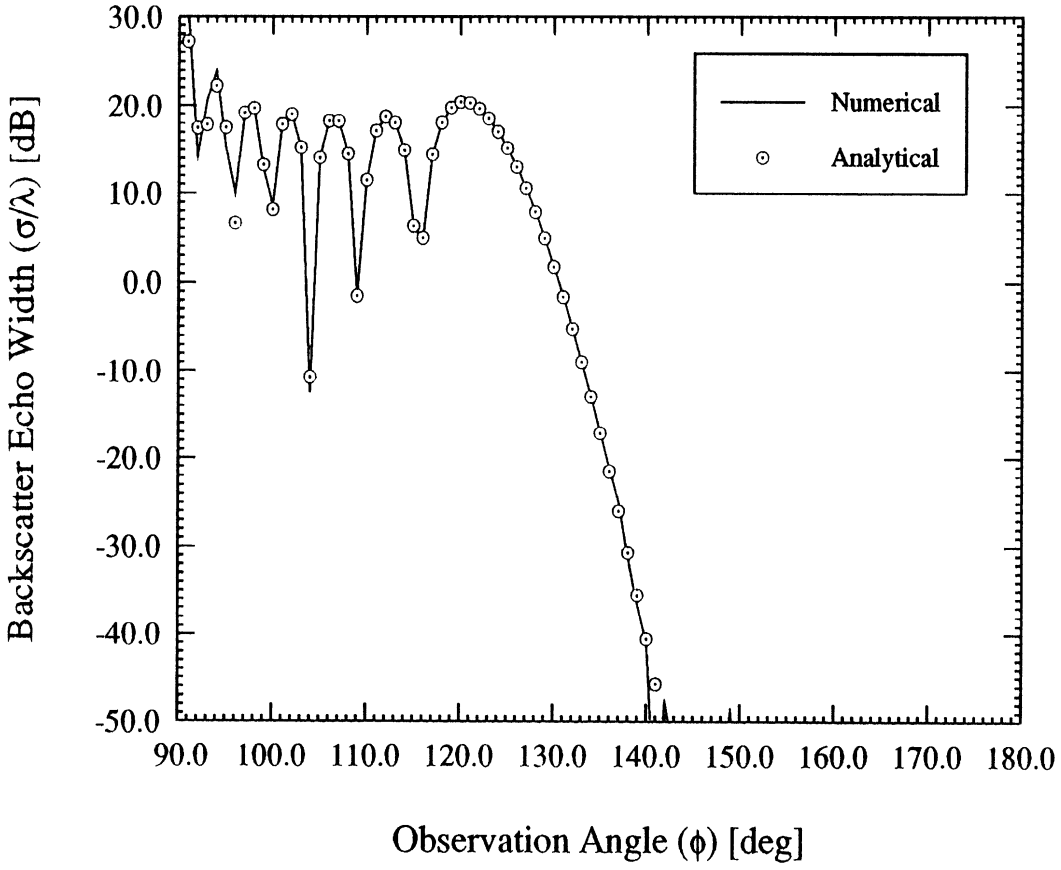

Figure 17. H-pol backscatter echowidth of the surface (see fig. 14).

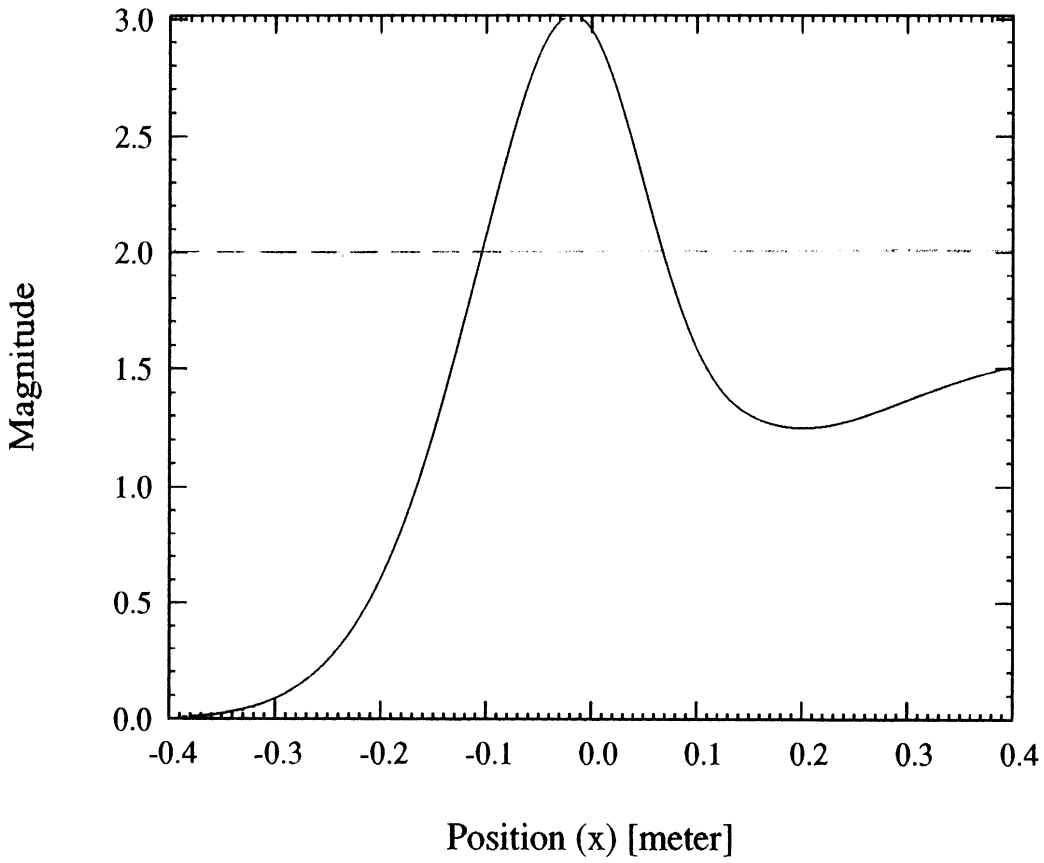

Figure 18. Current magnitude for S-shaped surface (see fig. 14) at grazing incidence and H-polarization (ignore results for $x > 0.1$ m)

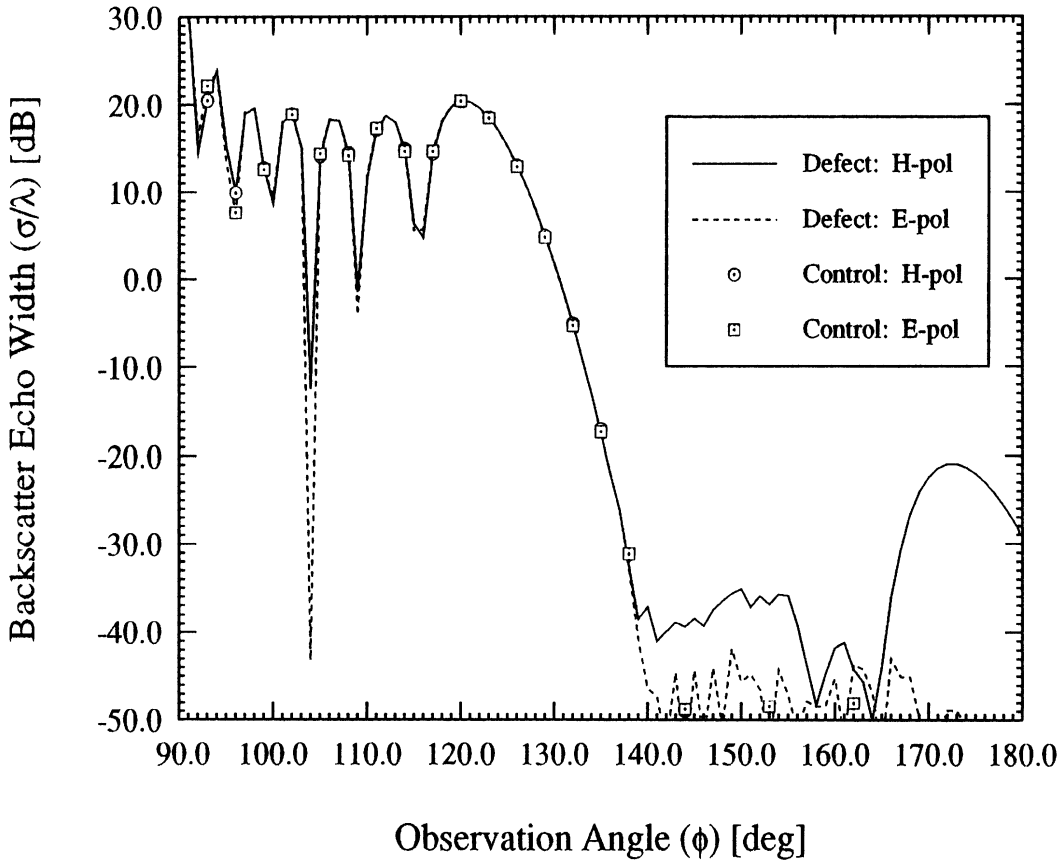

Figure 19. Backscatter echowidth of the surface (see fig. 14) with a defect placed at x = -6.8 cm for both E- and H-polarization.

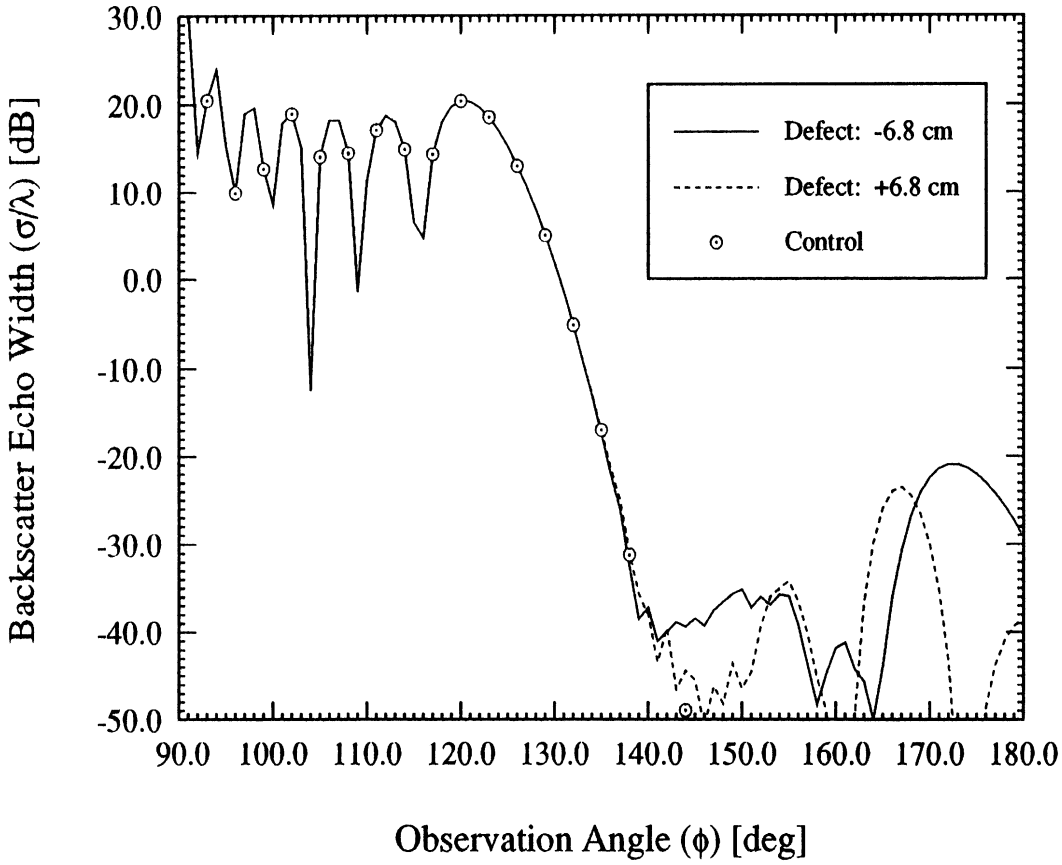

Figure 20. Backscatter echowidth of the surface (see fig. 14) with a defect placed at x = ± 6.8 cm for H-polarization.